Elastic properties of $CaCO_3$ high pressure phases from first principles*

Dan Huang(黄丹)[1], Hong Liu(刘红)[1,2,†], Ming-Qiang Hou(侯明强)[3], Meng-Yu Xie(谢梦雨)[4], Ya-Fei Lu(鹿亚飞)[1], Lei Liu(刘雷)[1], Li Yi(易丽)[1], Yue-Ju Cui(崔月菊)[1], Ying Li(李营)[1,2], Li-Wei Deng(邓力维)[4], and Jian-Guo Du(杜建国)[1]

[1] *CEA Key Laboratory of Earthquake Prediction (Institute of Earthquake Science), China Earthquake Administration (CEA), Beijing* 100036, *China*
[2] *National Key Laboratory of Shock Wave and Detonation Physics, Institute of Fluid Physics, China Academy of Engineering Physics, Mianyang* 621900, *China*
[3] *Center for High Pressure Science and Technology Advanced Research, Shanghai* 201203, *China*
[4] *Institute of Geology and Geophysics, Chinese Academy of Sciences, Beijing* 100029, *China*

(Received 3 January 2017; revised manuscript received 28 April 2017; published online 20 June 2017)

Elastic properties of three high pressure polymorphs of $CaCO_3$ are investigated based on first principles calculations. The calculations are conducted at 0 GPa–40 GPa for aragonite, 40 GPa–65 GPa for post-aragonite, and 65 GPa–150 GPa for the $P2_1/c$-h-$CaCO_3$ structure, respectively. By fitting the third-order Birch–Murnaghan equation of state (EOS), the values of bulk modulus K_0 and pressure derivative K_0' are 66.09 GPa and 4.64 for aragonite, 81.93 GPa and 4.49 for post-aragonite, and 56.55 GPa and 5.40 for $P2_1/c$-h-$CaCO_3$, respectively, which are in good agreement with previous experimental and theoretical data. Elastic constants, wave velocities, and wave velocity anisotropies of the three high-pressure $CaCO_3$ phases are obtained. Post-aragonite exhibits 25.90%–32.10% V_P anisotropy and 74.34%–104.30% V_S splitting anisotropy, and $P2_1/c$-h-$CaCO_3$ shows 22.30%–25.40% V_P anisotropy and 42.81%–48.00% V_S splitting anisotropy in the calculated pressure range. Compared with major minerals of the lower mantle, $CaCO_3$ high pressure polymorphs have low isotropic wave velocity and high wave velocity anisotropies. These results are important for understanding the deep carbon cycle and seismic wave velocity structure in the lower mantle.

Keywords: $CaCO_3$, elastic properties, wave velocity anisotropy, first principles

PACS: 91.60.Ba, 62.50.–p, 87.19.rd **DOI:** 10.1088/1674-1056/26/8/089101

1. Introduction

Carbonate is a dominant carbon-bearing material in the Earth's crust, mainly in pelagic marine sediment which can be delivered into the deep mantle by the subduction of oceanic crust and sediments.[1] Owing to the low solubility of carbon in mantle silicate, carbon is mainly stored in a separate phase which might be carbonate.[2] Thermodynamic models indicated that carbonates are stable during cold subduction.[3] An inclusion in ultra-deep diamonds, with $CaCO_3$, ferropericlase, perovskites, stishovite and others lower mantle minerals component, suggested that these carbonates stably exist in the lower mantle.[4,5] To understand the global carbon cycle on a geologic scale, it is necessary to study the stability, structure and elastic property of carbonate under high pressure.[6]

Calcite is the most stable $CaCO_3$ phase under ambient conditions and there have been a lot of reports about structures and thermodynamic properties.[7–10] Calcite transforms into aragonite in the upper mantle conditions.[11–13] Aragonite, considered to be stable in the mantle for a long time, was regarded as the main carbon-bearing phase in the Earth's interior. Recently, reports asserted the phase transformation from aragonite to a new structure of calcium carbonate at about 40 GPa.[14,15] The new phase has orthorhombic symmetry (*Pmmn*) and remains stable at least up to 86 GPa, named post-aragonite.[14] Besides, at about 130 GPa–140 GPa, experimental and theoretical studies found that a pyroxene-type structure $CaCO_3$ ($C222_1$) with a chain of CO_4^{4-} tetrahedron becomes more stable than post-aragonite, which could persist up to 192 GPa.[15,16] Furthermore, Pickard and Needs[17] thought that a new $CaCO_3$ structure with space group $P2_1/c$-h and chain of CO_4^{4-} tetrahedron, are more stable than $C222_1$ above 67 GPa. The discovery of these new $CaCO_3$ high pressure structures has attracted considerable attention to rethink the role of $CaCO_3$ in the carbon cycle. However, after the post-aragonite, $C222_1$ and $P2_1/c$-h structures are found, elastic properties of $CaCO_3$ at high pressures are rarely studied, and the $CaCO_3$ high-pressure structures have been controversial.

First-principle calculations are widely used to study the structural, electronic, elastic and thermodynamic properties, and phase transition of minerals.[18–21] In this study, we investigate the stability and elastic properties of aragonite, post-aragonite and the $P2_1/c$-h-$CaCO_3$ structure at high pressure up to 150 GPa with first-principle calculations. We show results and discussion of a full set of elastic constants, wave ve-

*Project supported by the National Natural Science Foundation of China (Grant Nos. 41174071, 41373060, 41374096, and 41403099) and the Seismic Fund of Institute of Earthquake Science, China Earthquake Administration (CEA) (Grant Nos. 2012IES0408, 2014IES0407, and 2016IES0101).

†Corresponding author. E-mail: liuhong_2006@hotmail.com

© 2017 Chinese Physical Society and IOP Publishing Ltd

locity and velocity anisotropies, which are important for understanding a carbon reservoir and the role of carbon in the deep mantle.

2. Calculation method

First-principle calculations are based on the density functional theory (DFT) incorporated with ultrasoft pseudopotential technique,[22] as implemented in the CASTEP code.[23] General gradient approximation (GGA) with the Perdew, Burke, and Ernzerhof (PBE) functional was employed to describe the exchange-correlation interaction.[24] A convergence of the plane-wave expansion was obtained with a cut-off of 450 eV for all calculations. Brillouin zone sampling was performed by the Monkhorst–Pack scheme. The k mesh was $6\times6\times6$ for all calculations.

The structures of aragonite, post-aragonite and $P2_1/c$-h-$CaCO_3$ adopted for this study possessed orthorhombic, orthorhombic and monoclinic symmetries with space groups $Pnma$, $Pmmn$, and $P2_1/c$-h, respectively. Simulations were performed at external pressures of 0 GPa–40 GPa for aragonite, 40 GPa–65 GPa for post-aragonite, and 65 GPa–150 GPa for $P2_1/c$-h-$CaCO_3$, respectively. The lattice constants and the atomic coordinates were simultaneously optimized under given pressures.

The stress tensor on the unit cell of a crystal structure can be directly calculated from the stress theorem[25] within the ultrasoft pseudopotential framework. At each pressure, a full set of elastic constants was computed by the homogeneous deformation method.[26] The full elastic constant tensors of orthorhombic and monoclinic structures have nine and thirteen independent components, respectively. Taking the Voight–Reuss–Hill average of simulated elastic constants and density, we determined the values of their bulk modulus (K), shear modulus (G), compressional (V_P), and shear (V_S) wave velocity according to the following equations,[27]

$$V_P=\sqrt{\frac{3K+4G}{3\rho}},\quad V_S=\sqrt{\frac{G}{\rho}}. \tag{1}$$

3. Results and discussion

The lattice constants and the atomic coordinates are simultaneously optimized under given pressures. For aragonite, full optimization of the unit-cell yields lattice parameters of $a=5.002$ Å, $b=8.014$ Å, $c=5.792$ Å at 0 GPa, which are in excellent agreement with previous experimental and theoretical results.[28,29] The average deviation is smaller than 1%. For post-aragonite, the calculated unit-cell parameters are $a=4.062$ Å, $b=4.592$ Å, $c=3.988$ Å at 66.4 GPa and $a=3.873$ Å, $b=4.451$ Å, $c=3.879$ Å at 110 GPa, respectively, which are in good accord with the results by Oganov, *et al.*[15] and Ono, *et al.*[14] The deviation is only about 1%–2%. Overall, our simulation schemes are efficient and in general agreement with the existing experimental data and theoretical data.

To investigate the phase stabilities and phase transition pressures of three polymorphs of $CaCO_3$, the relative enthalpy (to post-aragonite) and pressure curves are plotted in Fig. 1. According to the principle of thermodynamics, the structure with the lower energy is more stable. From Fig. 1, we find that the post-aragonite phase becomes more stable than aragonite above 40 GPa, which is consistent with previous DFT simulation and experiment results (Oganov, *et al.*[15] and Ono, *et al.*[14]). The $P2_1/c$-h-$CaCO_3$ becomes more stable than post-aragonite and $C222_1$-$CaCO_3$ above 65 GPa, in accord with the 67 GPa.[17] Consequently, our calculations were conducted at 0 GPa–40 GPa for aragonite, 40 GPa–65 GPa for post-aragonite, and 65 GPa–150 GPa for $P2_1/c$-h-$CaCO_3$, respectively.

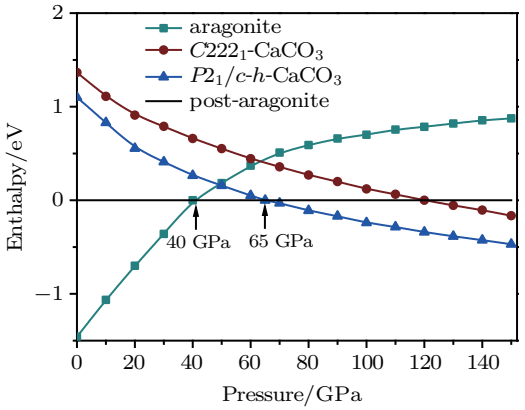


Fig. 1. (color online) Variations of calculated enthalpy difference relative to the post-aragonite phase with pressure.

According to calculated pressures and volume data of the three phases, we obtain their equations-of-state (EOS) parameters (equilibrium volume V_0, bulk modulus K_0, and its pressure derivative K_0') by fitting the third-order Birch–Murnaghan equation. The fitted parameters are shown in Table 1. For aragonite, the three fitted parameters are $V_0=232.50$ Å^3, $K_0=66.09$ GPa, and $K_0'=4.64$, respectively, which are in agreement with those presented by Li *et al.*[29] and Ono *et al.*[14] If K_0' is fixed at 4, the fitting yields results of $V_0=231.83$ Å^3 and $K_0=71.42$ GPa, which are in excellent agreement with data obtained by Fisler *et al.*,[30] and are slightly larger than the K_0 value of 65.4 reported by Martens *et al.*[31] A linear fit to the axial ratios a/a_0, b/b_0, c/c_0 versus pressure yields the linear axial compressibility of aragonite: $\beta_0(a)=2.53\times10^{-3}$ GPa^{-1}, $\beta_0(b)=3.66\times10^{-3}$ GPa^{-1}, and $\beta_0(c)=5.94\times10^{-3}$ GPa^{-1}, giving axial compressibility values in the order of $c>b>a$, indicating anisotropy in the compression behavior. These results are in consistence with previous studies.[29,30,32] For post-aragonite, with all parameters unrestrained, we obtain $V_0=106.44$ Å^3, $K_0=81.93$ GPa, $K_0'=4.49$ and if K_0' is fixed at 4, the fitted results are $V_0=101.76$ Å^3, $K_0=112.84$ GPa, close to the data of $V_0=98.3\pm1.9$ Å^3, $K_0=127\pm14$ GPa reported by

Ono *et al.*[14] Similarly, for $P2_1/c$-*h*-$CaCO_3$, $V_0 = 218.02$ Å^3, $K_0 = 56.55$ GPa, $K_0' = 5.40$ are obtained.

The complete elastic constants at given pressure for the three $CaCO_3$ structures are presented in Table 2 and Fig. 2. Under ambient conditions, the calculated longitudinal elastic constants of aragonite at 0 GPa are $C_{11} = 162.57$, $C_{22} = 107.81$, and $C_{33} = 96.48$ GPa. In comparison with the results presented by Liu *et al.*,[33] the average deviation is smaller than 3%. The order of $C_{11} > C_{22} > C_{33}$ shows the compression behaviors in different directions ($c > b > a$), which is consistent with the trend shown in the EOS parameters. At 40 GPa, the off-diagonal elastic constant C_{13} starts to fall. These changes might be a precursor of the phase transition (see Figs. 2(a)–2(c)).

Table 1. Calculated equations of state for aragonite, post-aragonite, and the $P2_1/c$-*h*-$CaCO_3$ at 0 K, and their comparisons with previous experimental and theoretical data.

	V_0/Å^3	K_0/GPa	K_0'	References
Aragonite	232.50	66.09	4.64	this study
	226.71(±0.01)	65.24(±0.24)	4.95(±0.12)	Li *et al.* (2015)[29]
	227.2(±1.0)	67.1(±6.3)	4.7(±0.8)	Ono *et al.* (2005)[14]
	233.84	66.9	4.48	Oganov *et al.* (2006)[15]
		64.8	4 (fixed)	Martinez *et al.* (1996)[32]
Post-aragonite	106.44	81.93	4.49	this study
	101.76	112.84	4 (fixed)	this study
	98.3(±1.9)	127(±14)	4 (fixed)	Ono *et al.* (2005)[14]
	109.74	90(±13)	4.94	Oganov *et al.* (2006)[15]
$P2_1/c$-*h*-$CaCO_3$	218.02	56.55	5.40	this study

Table 2. Calculated values of elastic constants C_{ij} (in unit GPa), bulk modulus, shear modulus (in unit GPa), and compressional (V_P) and shear (V_S) wave velocity (in units km/s) under pressure P (in unit GPa) at 0 K.

P	C_{11}	C_{22}	C_{33}	C_{44}	C_{55}	C_{66}	C_{12}	C_{13}	C_{23}	C_{15}	C_{25}	C_{35}	C_{46}	B	G	V_P	V_S
Aragonite																	
0	162.57	107.81	96.48	41.91	36.44	19.59	53.65	26.42	42.77					66.42	33.77	6.27	3.45
5	201.32	128.79	119.91	47.39	44.13	25.54	78.50	40.93	63.14					88.35	38.97	6.80	3.59
10	239.97	152.44	143.48	52.29	51.46	32.21	102.90	55.56	84.25					110.69	44.09	7.29	3.72
14	263.94	185.14	157.22	62.48	56.19	32.44	111.35	70.17	105.38					128.05	48.33	7.63	3.83
20	312.25	215.08	180.56	74.52	61.36	36.90	139.30	83.55	130.73					152.76	53.70	8.06	3.94
24	334.47	229.52	198.63	80.15	65.26	37.01	160.23	94.92	147.88					169.48	54.98	8.28	3.94
30	371.14	262.24	219.05	89.40	70.43	41.77	184.33	108.94	170.65					191.44	59.98	8.61	4.05
34	400.90	296.74	227.58	100.22	74.76	46.87	200.32	116.12	187.24					205.35	65.55	8.84	4.18
40	457.65	329.79	247.20	112.95	78.79	55.04	212.95	122.61	210.63					224.86	73.31	9.15	4.36
Post-aragonite																	
40	323.23	499.22	530.69	129.46	12.97	29.61	150.26	147.11	135.63					241.49	66.70	9.02	4.05
45	350.70	529.25	566.12	140.19	22.26	30.87	161.74	162.63	144.75					260.06	77.46	9.36	4.32
50	385.24	566.94	597.04	150.61	35.65	34.70	170.92	175.89	159.27					280.01	89.84	9.73	4.61
55	412.70	603.27	628.35	163.47	45.99	37.39	181.20	191.51	170.39					298.82	99.14	10.01	4.80
60	443.60	634.70	656.90	172.55	56.27	38.92	190.37	205.42	181.51					316.84	106.87	10.25	4.95
65	472.02	664.97	689.62	184.00	65.31	41.45	199.22	218.17	194.76					334.72	114.78	10.48	5.09
$P2_1/c$-*h* $CaCO_3$																	
65	528.33	565.99	498.62	176.11	128.79	241.78	330.70	230.85	284.15	5.52	87.17	20.24	88.97	357.98	143.17	11.02	5.63
70	556.73	592.27	525.20	187.19	132.75	253.18	348.42	242.07	298.36	3.48	90.68	21.17	92.78	376.46	149.89	11.21	5.72
80	614.38	641.33	584.75	206.25	137.60	274.61	380.43	258.51	326.64	–1.40	98.10	22.97	99.38	411.89	162.29	11.56	5.87
90	673.46	692.77	643.53	226.45	139.38	295.44	412.16	275.92	355.43	–6.57	103.37	26.60	105.54	447.72	174.33	11.89	6.02
100	722.95	743.72	698.74	246.39	147.26	315.62	442.93	293.73	384.27	–11.61	110.90	26.65	111.45	482.33	186.46	12.19	6.15
110	782.50	791.06	755.15	263.61	152.51	334.59	472.16	310.53	411.07	–17.06	118.57	27.70	117.19	516.63	197.81	12.46	6.28
120	837.02	843.38	816.30	283.77	157.18	355.40	503.21	326.24	438.14	–23.12	123.97	31.06	122.48	551.64	210.27	12.75	6.41
130	893.83	891.81	873.65	302.20	161.59	373.25	532.08	340.83	464.49	–29.11	130.96	32.40	127.28	585.19	221.26	13.00	6.52
140	947.71	937.33	932.83	320.94	164.31	389.70	557.89	356.32	491.30	–32.61	137.77	33.11	132.68	617.88	231.59	13.22	6.61
150	1004.04	981.80	993.82	338.71	170.45	407.72	586.19	370.76	516.13	–39.06	144.22	36.28	137.75	650.88	242.96	13.46	6.72

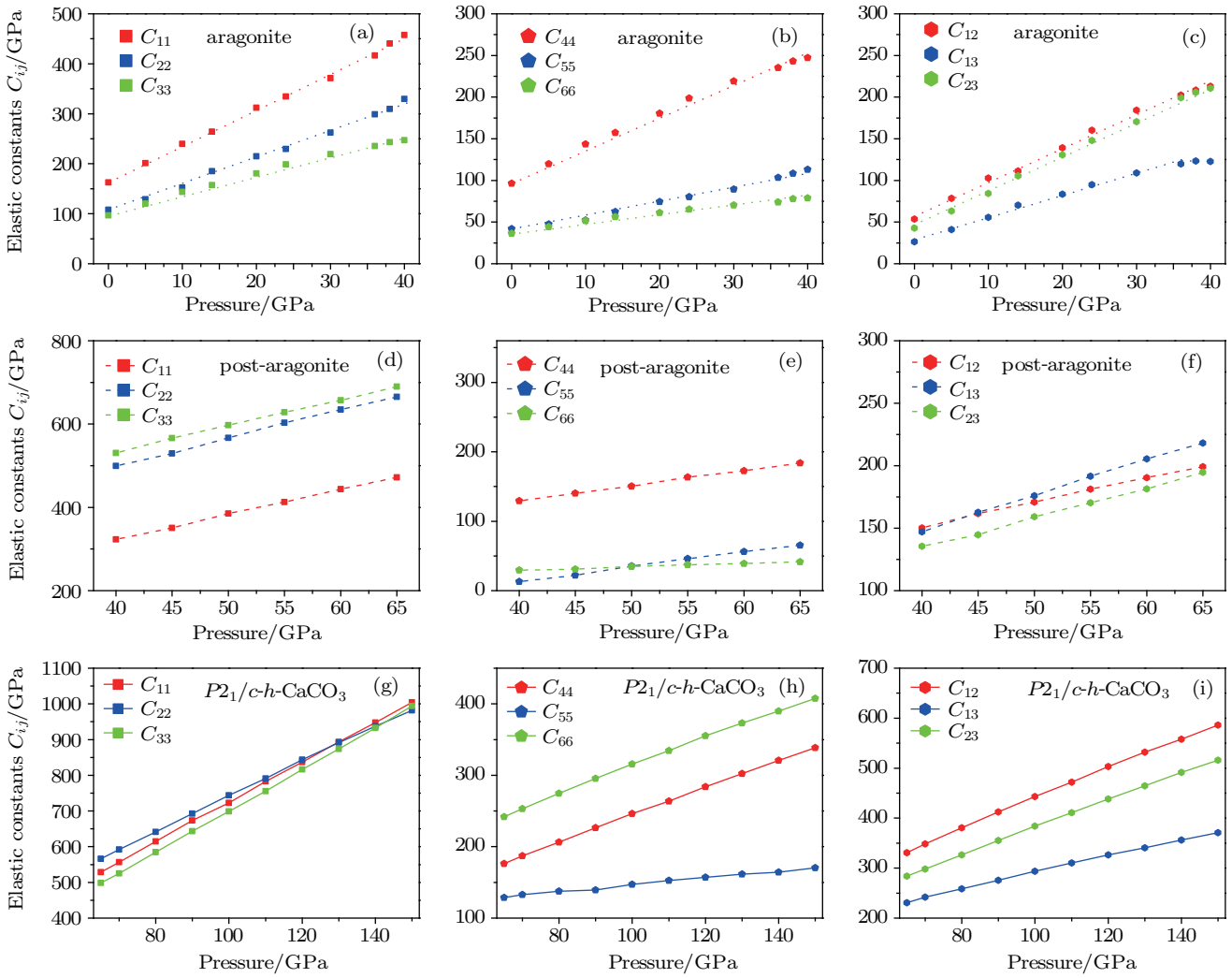


Fig. 2. (color online) Calculated elastic constants C_{ij} under given pressure for [(a)–(c)] aragonite, [(d)–(f)] post-aragonite, and [(g)–(i)] $P2_1/c$-h-$CaCO_3$.

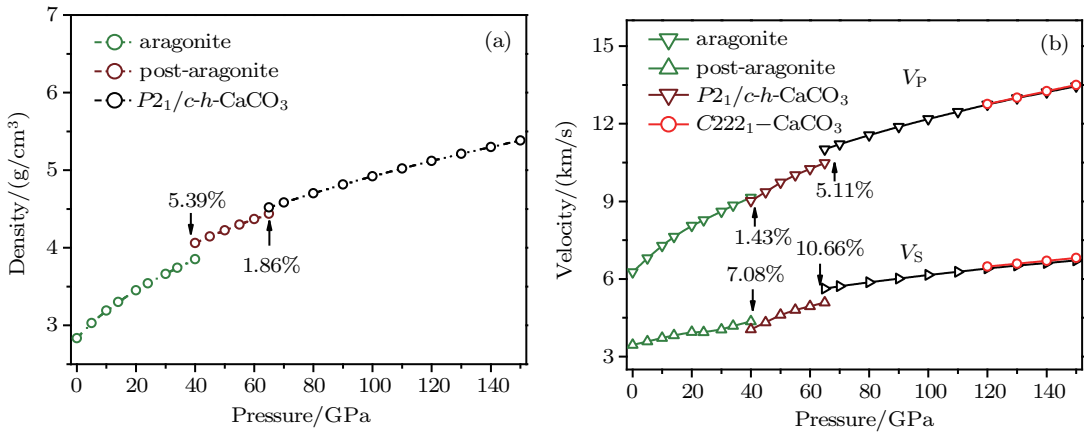


Fig. 3. (color online) Variations of calculated (a) densities and (b) wave velocities for aragonite, post-aragonite, $P2_1/c$-h-$CaCO_3$, $C222_1$-$CaCO_3$ with pressure.

In the post-aragonite phase, the elastic constants exhibit a different behavior from that of aragonite. The C_{22} and C_{33} of post-aragonite are almost the same and both of them are larger than C_{11} in the entire pressure range (40 GPa–65 GPa). It indicates that the a axis of post-aragonite is more compressible than b and c axes. The compression results reflect the characteristic of layered mineral that this structure is more compressive in the direction perpendicular ([100] directions here in this work) to the layers (layers parallel to the [001] and [010] directions) (see Figs. 2(d)–2(f)).

For $P2_1/c$-h-$CaCO_3$, the values of C_{11}, C_{22}, and C_{33} are close at 65 GPa–150 GPa, implying that a, b, and c axes have similar compression behaviors. The shear elastic constants and off-diagonal elastic constants of $P2_1/c$-h-$CaCO_3$

increase smoothly with pressure and show different sizes with $C_{66} > C_{44} > C_{55}$ and $C_{12} > C_{23} > C_{13}$, respectively. Compared with post-aragonite at 65 GPa, $P2_1/c$-h-$CaCO_3$ exhibits smaller longitudinal elastic constants except C_{11} and larger off-diagonal and shear elastic constants except C_{44} (see Figs. 2(g)–2(i)). The differences in density, V_P and V_S discontinuities between aragonite and post-aragonite at 40 GPa are 5.39%, 1.43%, and 7.08%, respectively.

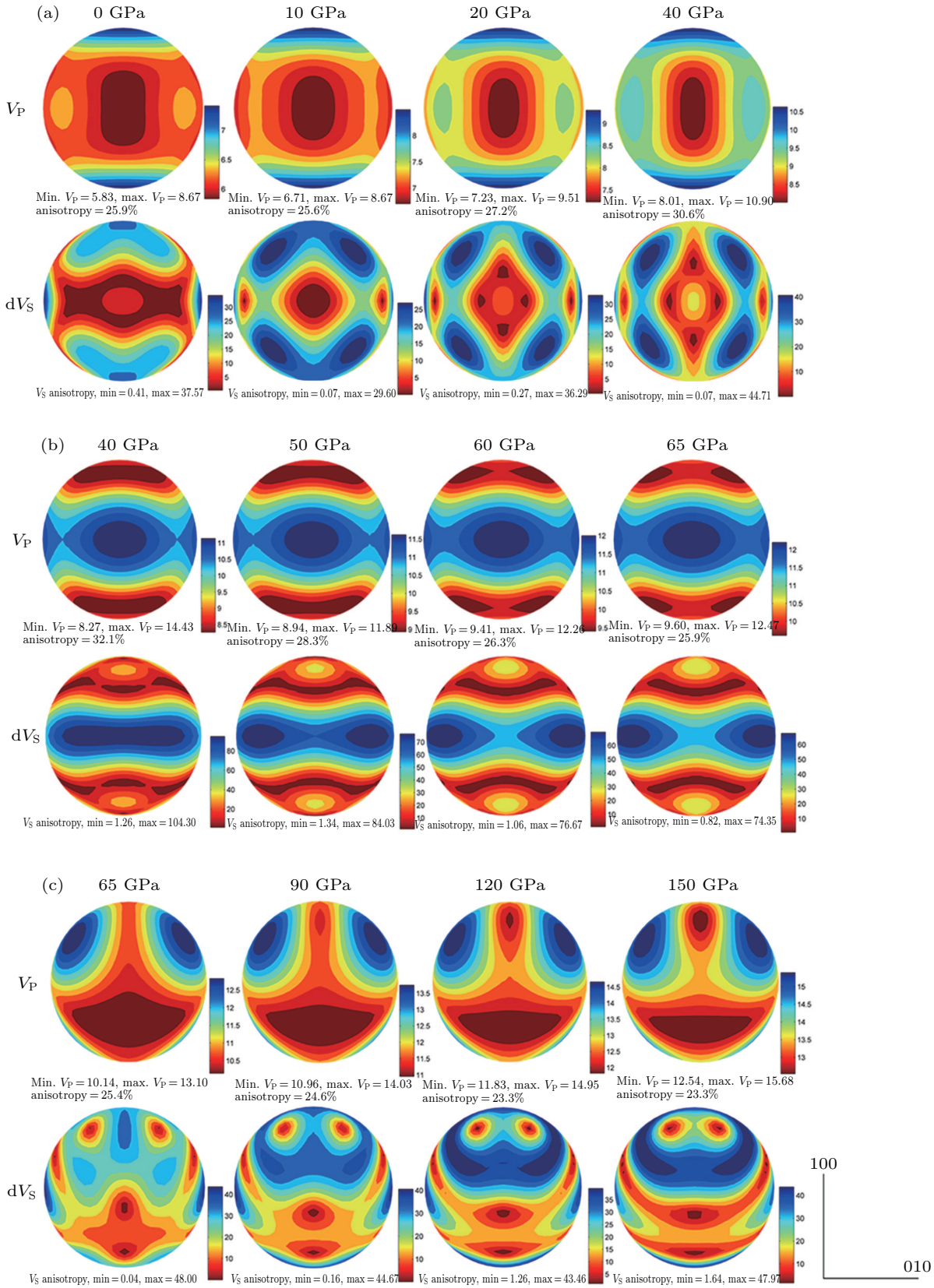


Fig. 4. (color online) Calculated profiles of V_P anisotropy and shear wave splitting (dV_S) of (a) aragonite, (b) post-aragonite, (c) $P2_1/c$-h-$CaCO_3$ with pressures by using the calculated elastic constants.

The density discontinuity is in good accord with the result given by Oganov *et al.*,[15] and those density, V_P and V_S discontinuities at 65 GPa between post-aragonite and $P2_1/c$-*h*-$CaCO_3$ are 1.86%, 5.11%, and 10.66%, respectively. The huge density increase, with relatively small bulk and shear modulus differences, leads to smaller acoustic velocities of post-aragonite. Besides, larger acoustic velocities appear in $P2_1/c$-*h*-$CaCO_3$ and $C222_1$-$CaCO_3$ so that the two phases have a chained structure and almost similar acoustic velocities. It indicates that the polymerization of CO_4^{4-} tetrahedron, leading a more compact structure, can increase the acoustic velocity of $CaCO_3$ (see Fig. 3).

Single crystal wave velocities in various crystallographic directions are determined by Christoffel's equation[34]

$$\left|C_{ijkl}n_jn_l - \rho V^2\delta_{ik}\right| = 0, \tag{2}$$

where C_{ijkl}, ρ, n, V, and δ_{ik} are elastic constants, density, propagation, wave velocity, and Kronecker delta, respectively.

Figure 4 shows the acoustic wave velocities of three structures along different crystalline directions. For aragonite, P-wave propagates fastest in the [100] direction and slowest in the [001] direction. Whereas, the P-wave velocity of post-aragonite is the fastest in the [001] and [010] direction, and slowest in the [110] direction. $P2_1/c$-*h*-$CaCO_3$ propagates fastest in the [111] direction, and slowest in the direction [$\bar{1}$01]. These results are in agreement with the orders of elastic constants $C_{11} > C_{22} > C_{33}$ for aragonite, $C_{22} \approx C_{33} > C_{11}$ for post-aragonite, and $C_{11} \approx C_{22} \approx C_{33}$ for $P2_1/c$-*h*-$CaCO_3$. Moreover, the largest shear wave splitting (dV_S) directions switch from [010] to [111] for aragonite at about 10 GPa, from [001] to [011] for post-aragonite at about 50 GPa, and from [010] to [111] at about 120 GPa for $P2_1/c$-*h*-$CaCO_3$, respectively. It means that when the transition occurs, the fastest propagation direction of the P-wave and the splitting direction of the largest shear wave are changed. Meanwhile, these changes also reflect structural changes from a block structure of aragonite to a layered structure of post-aragonite and to a chained structure of $P2_1/c$-*h*-$CaCO_3$.

Azimuthal anisotropy values (A_P, A_S) for P and S waves at different pressures are defined as

$$A_P = \frac{2(V_P^{max} - V_P^{min})}{V_P^{max} + V_P^{min}}, \tag{3}$$

$$A_S = \frac{2\max(V_{S1} - V_{S2})}{V_S^{max} + V_S^{min}}, \tag{4}$$

where V_P^{max}, V_P^{min}, V_S^{max}, and V_S^{min} are the maxima and minima of V_P and V_S velocities, respectively. The V_{S1} and V_{S2} are two orthogonally polarized V_S velocities, and $\max(V_{S1} - V_{S2})$ is the maximum difference between V_{S1} and V_{S2} along the same direction of propagation. Figure 5(a) shows azimuthal anisotropies for P and S waves of three $CaCO_3$ phases at given pressure. There are strong shear anisotropies in carbonates especially for post-aragonite and $P2_1/c$-*h*-$CaCO_3$. Aragonite exhibits 25.60%–30.60% V_P anisotropy and 29.60%–44.92% V_S anisotropy. With pressure increasing, the A_S of aragonite first decreases under pressure lower than 10 GPa and then increases under pressure of 10 GPa–40 GPa. The A_S minimum of 29.6% is present in aragonite at 10 GPa. The post-aragonite phase has abnormally high A_S anisotropy. At pressure in a range of 40 GPa–65 GPa, post-aragonite exhibits 25.90%–32.10% V_P anisotropy and 74.34%–104.30% V_S splitting anisotropy. The triangular CO_3^{2-} units lead to anisotropy of elastic properties of aragonite and post-aragonite. Especially for post-aragonite, the CO_3^{2-} units show a layered distribution, which further increases the anisotropy up to 104.30%. The As of post-aragonite presents a sharp decrease at 40 GPa and subsequently keeps falling up to 65 GPa. It may be caused by the decreasing of layer distance with pressure increasing (Fig. 5(b)). The $P2_1/c$-*h*-$CaCO_3$ shows a 22.30%–25.40% V_P anisotropy and a 42.81%–48.00% V_S anisotropy. This means that the phase transition leads to small changes in elastic velocity but abnormally large changes in the elastic anisotropies, especially for shear wave anisotropies.

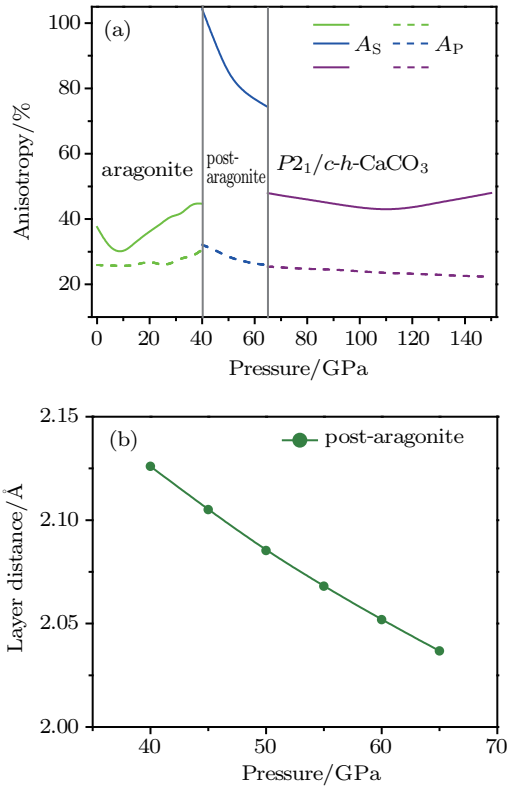


Fig. 5. (color online) (a) Variations of calculated azimuthal anisotropy for *P* (A_P) and *S* (A_S) waves of aragonite (green), post-aragonite (blue), and $P2_1/c$-*h*-$CaCO_3$ (purple) with pressure. (b) Variation of calculated layer distance of post-aragonite with pressure.

Figures 6 and 7 show the comparisons of shear anisotropy and isotropic wave velocities among the three carbonate phases, and other mantle minerals: $MgSiO_3$ perovskite (Mg–Pv), post-perovskite (Mg–PPv), $CaSiO_3$ perovskite (Ca–Pv), (Mg, Fe)O ferropericlase (Fp), calcium ferrite-type $MgAl_2O_4$ (CF) and new hexagonal aluminous (NAL) phase.[35–38]

Clearly, $CaCO_3$ high pressure polymorphs have higher wave velocity anisotropies and lower wave velocity than silicate mineral and other carbonate in the whole pressure range. At high pressures, the velocity of $CaCO_3$ are less than PREM till the outer core pressure, which means that the existence of $CaCO_3$ could shed light on the low velocity region in the deep mantle, especially the bottom of the lower mantle.

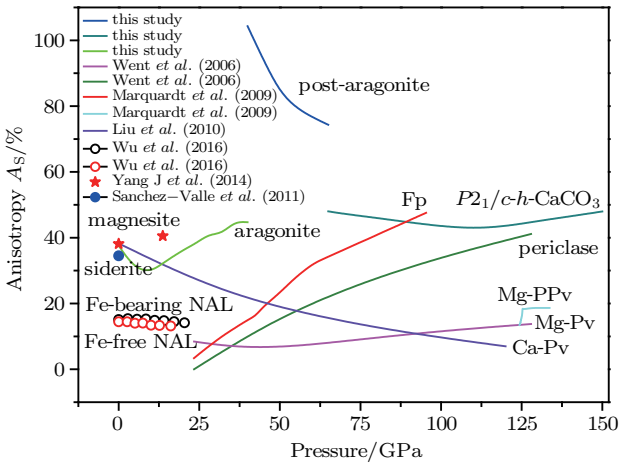


Fig. 6. (color online) (a) Variations of azimuthal anisotropy for shear wave of aragonite, post-aragonite, and $P2_1/c$-h-$CaCO_3$ (this study) with pressure, compared with those of magnesite,[39] siderite,[40] periclase (MgO), and Mg-Pv,[41] Fp and Mg-PPv,[42] Ca-Pv,[43] and Fe-bearing and Fe-free NAL.[44]

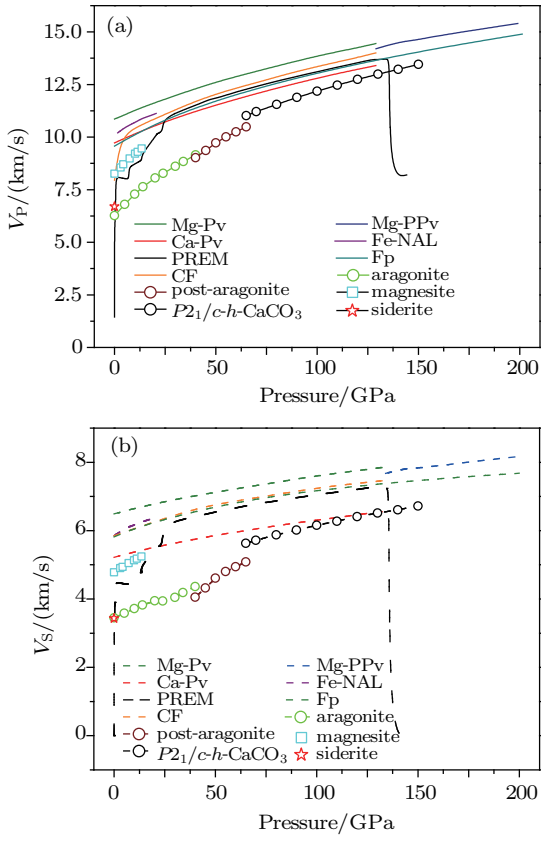


Fig. 7. (color online) Comparisons of (a) V_P and (b) V_S between carbonates and other major candidate minerals of subducted basalt at high pressure. The values from the PREM model were also plotted for comparison. Circle: $CaCO_3$ (this study); blue square: magnesite;[39] red pentacle: Siderite;[40] olivine: Mg–Pv;[45] red: Ca–Pv;[46] purple: Fe-NAL phase;[44] royal: Mg–PPv;[47] orange: CF phase;[48] black: PREM.[49]

4. Conclusions

In summary, stabilities and elastic properties of three high pressure polymorphs of $CaCO_3$ are investigated based on first principles calculations. Calculations are conducted at 0 K and 0 GPa–40 GPa for aragonite, 40 GPa–65 GPa for post-aragonite, and 65 GPa–150 GPa for $P2_1/c$-h-$CaCO_3$, respectively. By fitting the third-order Birch–Murnaghan equation of state, the values of bulk modulus and pressure derivative are 66.09 GPa and 4.64 for aragonite, 81.93 GPa and 4.49 for post-aragonite, 56.55 GPa and 5.40 for $P2_1/c$-h-$CaCO_3$, respectively, which are in excellent agreement with previous experimental and theoretical data. A full set of elastic constants, acoustic velocities and anisotropy of the three high-pressure $CaCO_3$ phases is investigated. High shear anisotropy and low acoustic velocities are presented in three $CaCO_3$ high pressure phases. These results could have very important geophysical significance for ascertaining the chemical composition and velocity structure of the Earth's lower mantle.

Acknowledgments

Calculations were performed at the Supercomputer Group of the Institute of Earthquake Science, China Earthquake Administration.

References

[1] Becker H and Altherr R 1992 *Nature* **358** 745
[2] Keppler H, Wiedenbeck M and Shcheka S S 2003 *Nature* **424** 414
[3] Kerrick D M and Connolly J A 2001 *Nature* **411** 293
[4] Brenker F E, Vollmer C, Vincze L, Vekemans B, Szymanski A, Janssens K, Szaloki I, Nasdala L, Joswig W and Kaminsky F 2007 *Earth Planet. Sci. Lett.* **260** 1
[5] Kaminsky F, Wirth R, Matsyuk S, Schreiber A and Thomas R 2009 *Mineral. Mag.* **73** 797
[6] Dasgupta R and Hirschmann M M 2010 *Earth Planet. Sci. Lett.* **298** 1
[7] Salje E and Viswanathan K 1976 *Contrib. Mineral. Petrol.* **55** 55
[8] Wolf G, Königsberger E, Schmidt H, Königsberger L C and Gamsjäger H 2000 *J. Therm. Anal. Calorim.* **60** 463
[9] Ivanov B A and Deutsch A 2002 *Phys. Earth Planet. In.* **129** 131
[10] Catalli K and Williams Q 2005 *Am. Mineral.* **90** 1679
[11] Jamieson J C 1953 *J. Chem. Phys.* **21** 1385
[12] Boettcher A and Wyllie P 1968 *J. Geol.* **76** 314
[13] Suito K, Namba J, Horikawa T, Taniguchi Y, Sakurai N, Kobayashi M, Onodera A, Shimomura O and Kikegawa T 2001 *Am. Mineral.* **86** 997
[14] Ono S, Kikegawa T, Ohishi Y and Tsuchiya J 2005 *Am. Mineral.* **90** 667
[15] Oganov A R, Glass C W and Ono S 2006 *Earth Planet. Sci. Lett.* **241** 95
[16] Ono S, Kikegawa T and Ohishi Y 2007 *Am. Mineral.* **92** 1246
[17] Pickard C J and Needs R J 2014 *Phys. Rev. B* **91** 104101
[18] Liu B, Wang X J and Bu X Y 2016 *Acta Phys. Sin.* **65** 126102 (in Chinese)
[19] Yu Y, Liu D J, Wu R X 2016 *Acta Phys. Sin.* **65** 027101 (in Chinese)
[20] Lu Q, Zhang H Y, Cheng Y, Cheng X Y and Ji G F 2016 *Chin. Phys. B* **25** 348
[21] Wang J F, Fu X N, Zhang X D, Wang J T, Li X D and Jiang Z Y 2016 *Chin. Phys. B* **25** 086302
[22] Vanderbilt D 1990 *Phys. Rev. B* **41** 7892

[23] Clark S J, Segall M D, Pickard C J, Hasnip P J, Probert M J, Refson K and Payne M C 2005 *Z. Kristallogr.* **220** 567
[24] Perdew J P, Burke K and Ernzerhof M 1996 *Phys. Rev. Lett.* **77** 3865
[25] Nielsen O H and Martin R M. 1983 *Phys. Rev. Lett.* **50** 697
[26] Mariani M, Sharp N D and Walmsley S H 1996 *Chem. Phys.* **204** 1
[27] Watt J P 1979 *J. Appl. Phys.* **50** 6290
[28] Dickens B and Bowen J 1971 *J. Res. Natl. Bur. Stand. A Phys. Chem.* **75** 27
[29] Li Y, Zou Y, Chen T, Wang X, Qi X, Chen H, Du J and Li B 2015 *Am. Mineral.* **100** 2323
[30] Fisler D K, Gale J D and Cygan R T 2000 *Am. Mineral.* **85** 217
[31] Martens R, Rosenhauer M and Gehlen K 1982 *High-Pressure Researches in Geoscience* (Stuttgart: Schreyer W Education) pp. 215–222
[32] Martinez I, Zhang J and Reeder R J 1996 *Am. Mineral.* **81** 611
[33] Liu L G, Chen C C, Lin C C and Yang Y J 2005 *Phys. Chem. Miner.* **32** 97
[34] Musgrave M J 1970 *J. Crystal Acoustics* (Boca Raton: Holden-Day) p. 288
[35] Ono S, Ito E and Katsura T 2001 *Earth Planet. Sci. Lett.* **190** 57
[36] Hirose K, Takafuji N, Sata N and Ohishi Y 2005 *Earth Planet. Sci. Lett.* **237** 239
[37] Akaogi M, Hamada Y, Suzuki T, Kobayashi M and Okada M 1999 *Phys. Earth Planet. In.* **115** 67
[38] Maruyama S, Santosh M and Zhao D 2007 *Gondwana Res.* **11** 7
[39] Yang J, Mao Z, Lin J F and Prakapenka V B 2014 *Earth Planet. Sci. Lett.* **392** 292
[40] Sanchez-Valle C, Ghosh S and Rosa A D 2011 *Geophys. Res. Lett.* **38** 422
[41] Wenk H R, Speziale S, McNamara A and Garnero E 2006 *Earth Planet. Sci. Lett.* **245** 302
[42] Marquardt H and Garnero E J 2009 *Science* **324** 224
[43] Liu Z J, Duan S Q, Yan J, Sun X W, Zhang C R and Chu Y D 2010 *Solid State Commun.* **150** 943
[44] Wu Y, Yang J, Wu X, Song M, Yoshino T, Zhai S, Qin S, Huang H and Lin J F 2016 *J. Geophy. Res. Solid Earth* **121** 5696
[45] Murakami M, Sinogeikin S V, Hellwig H, Bass J D and Li J 2007 *Earth Planet. Sci. Lett.* **256** 47
[46] Tsuchiya T 2011 *Phys. Earth Planet. In.* **188** 142
[47] Taku T, Jun T, Koichiro U and Wentzcovitch R M 2004 *Geophys. Res. Lett.* **31** 189
[48] Dai L, Kudo Y, Hirose K, Murakami M, Asahara Y, Ozawa H, Ohishi Y and Hirao N 2013 *Phys. Chem. Miner.* **40** 195
[49] Dziewonski A M and Anderson D L 1981 *Phys. Earth Planet. In.* **25** 297